EGYPTIAN DENTAL JOURNAL
www.eda-egypt.org
VOL. 71, 1189:1199, APRIL, 2025
PRINT ISSN 0070-9484 • ONLINE ISSN 2090-2360
ORAL SURGERY
Submit Date : 22-12-2024 • Accept Date : 13-01-2025 • Available online: 01-04-2025 • DOI : 10.21608/edj.2025.346818.3319

NECROSIS RELATED TO CHROMATIC ANALYSIS OF MEDIAN FOREHEAD FLAP

Mohammed Hassan Al Kabany* *and* Reda A. Nofal**

ABSTRACT

Objective: The current study was directed to analyze the vascularity of different parts of median forehead flaps using chromatic analyses.

Patients and methods: Eight patients were included in the study. Following basal cell carcinoma resection, the median forehead flap was created. A high-resolution visible light photograph was captured, including the flap and the adjacent donor site tissues. Split visible light color channels (Red, Green, and Blue) were measured for different regions of interest. The measured areas were the normal tissue, total flap, flap base, apex, margin, and flap center. Differences in visible color channels of these regions were calculated. The flap's dimensions were measured, including flap length, base width, and apex width. Flap base width to flap length and flap apex width to flap base width ratios were calculated. In the first postoperative month, another photograph was taken to measure the flap necrosis percentage at the reconstruction site. The relation of the flap necrosis percentage with the calculated differences and ratios was estimated.

Results: There were strong significant correlations between flap necrosis percentage and the difference between flap base and flap apex red and green channels' values, flap base width to flap length ratio, and flap base width to flap apex width ratio. Significant practical differences existed between the flap base to apex and the flap center to margins RGB channels.

Conclusion: To the limitation of the current study, the reduction of flap apex width and flap length relative to flap base width reduces flap necrosis percentage.

KEYWORDS: Median forehead flap; Flap necrosis; chromatic analysis; visible light channels; flap dimensions

* Department of Oral and Maxillofacial Surgery, Faculty of Dentistry, Cairo University, Egypt.
Department of Oral and Maxillofacial Surgery, Faculty of Dentistry, Umm Al-Qura University, KSA
** Professor of Oral and Maxillofacial Surgery, Faculty of Dental Medicine & Al-Azhar University

INTRODUCTION

Grafts and flaps are the cornerstone in reconstructing facial defects following malignant neoplasm excision.[1] The most common non-melanotic skin malignant tumor affecting the exposed regions of the head and neck is basal cell carcinoma.[2,3] Basal cell carcinoma is a slowly growing tumor of low mortality but of high morbidity. The neoplasm invades and destructs local tissues and requires wide surgical excision.[4] Minor defects could be closed with local advancement or rotational flaps. However, skin reconstruction is indicated in medium to large-sized defects.[5] Facial skin reconstruction could be done with pedicled or free vascularized flaps.

Despite the advancement of free graft techniques, pedicled flaps are still used in facial reconstruction. Mahieu et al. compared the reconstruction of head and neck defects using free versus pedicled flaps, indicating equal functional outcomes and complications.[6] Moreover, the esthetic demands in facial reconstruction necessitate the exact matching of the graft to the neighboring skin. Forehead flaps have a tint and texture that precisely matches the skin of the face and nose.[7] Thus, forehead pedicled flaps are commonly used to reconstruct nasal, orbital, and cheek skin.

There are several forehead-pedicled flaps, including median, paramedian, and midline. The median design is the original forehead flap with a broad pedicle gaining blood supply mainly from both supratrochlear arteries, thus preserved for more significant defects.[8] The median flap was modified to narrow the pedicle to be based on one supratrochlear artery and run lateral to the midline, creating the paramedian flap. The midline flap has a narrow pedicle based on one supratrochlear artery like the paramedian flap and extents in the midline like the median one. [9-11]

The major complication of pedicled skin flaps is tissue necrosis.[12] Tissue necrosis is related primarily to arterial and venous insufficiency.[13] Several techniques were used to determine vascularity insufficiency in free and pedicled flaps. These techniques include near-infrared spectroscopy, hand-held Doppler probe, surface temperature estimation, pulse oximetry, laser Doppler flowmetry, and implantable Doppler ultrasound probe.[14-20] However, being expensive and having high technology demands, conventional clinical observation methods are preferred. Conventional clinical observation methods include skin color inspection, flap surface temperature, capillary refill time, and bleeding on puncture.[21] These clinical observation methods are fast, low-cost, and noninvasive.[22] Other methods were used in experimental work to evaluate flap vascularity based on the flap viable tissue percentage.[23-26] Measuring flap viable tissue percentage could be done using the weight of the paper template[26], paper template area[27], and photographic area. Photographic area can measure the percentage of necrosis areas to the total area of the flap.[28-30]

The color of the flap is considered the most consistent indicator of flap viability.[21,31] Hemoglobin and oxyhemoglobin in the blood are the main chromophores detected by visible light.[32-34] These chromophores allow the evaluation of blood perfusion of the flap by inspection.[35] However, flap color inspection is subjective and relies on surgeon experience.[21] Improving visible light image resolution, contrast, and comprehensive information established a reliable method to evaluate flap color.[22] Chromatic analysis of visible light color channels (RGB channels) of digital images allowed the evaluation of blood perfusion of the flaps.[35] Kiranantawat et al.[31] developed a smartphone application to assess the severity of vascularity occlusion of the free flaps. The application was initially calibrated by measuring the visible light color difference between the middle and index fingers after applying different occluding pressures around the index finger. The application

showed a sensitivity of 94% and specificity of 98% in detecting the degree of free flap vascular occlusion. Gu et al.[35] measured RGB and infrared light components on experimental flap ligation and de-ligation. The RGB channels were consistently related to reducing and reestablishing flap blood flow. These channels gradually reduced following continued ligation and recovered near the original levels following ligature release. On the other hand, there was no relation between the degree of ligation and the infrared component.

The ability of RGB channels to detect flap vascularity was directed to assess and improve free flap success rates.[22,31] However, this was not utilized in studying pedicled flap vascularity relative to flap design and degree of flap necrosis. Moreover, studying the vascularity of different regions of free and pedicled flaps using chromatic RGB analysis was not addressed. Chromatic RGB analysis could correlate flap design parameters to healing, allowing design modification to improve functional and esthetic outcomes.

To our knowledge, no study has been conducted addressing this point. The current study tries to bridge this gap and establish a base system for further research. The current study aimed to analyze the vascularity of different parts of the median forehead flaps utilizing RGB values. This analysis correlated flap design parameters and the degree of flap necrosis to establish a relation between flap design and the degree of flap necrosis.

PATIENTS AND METHODS

Patients' selection

The current prospective analytic study included patients with basal cell carcinoma requiring resection and reconstruction, utilizing a median forehead flap. The selected patients should have no systemic disorders that could affect flap healing. Black strips were applied to the patient's digital images to hide their identities. There was no specific intervention related to the research that required ethical approval.

Tumor resection:

Surgical tumor excision with a 5mm clinical safety margin was done for all patients. The excised tumors were marked with orientation stitches and sent for frozen section pathological examination. Resection was repeated according to the biopsy results till complete excision. The existing defect was enlarged to bring the future scar to lie with the borders of facial esthetic subunits. (Fig 1 (A))

Median forehead flap:

A template was made to transfer the shape of the defect to the forehead flap. The template was traced over the midline of the forehead and slightly shifted to the contralateral side to allow for more rotation arc and to minimize pedicle kinking. A suture material was used to confirm the reach of the designed flap to the defect. The incision was done to the subgaleal plane, leaving a pedicle over the supraorbital rim at the glabella. Dissection preceded in the subgaleal plane to the glabella. Periosteum was incised at the glabella level, and dissection proceeded subperiosteally to a level lower than the superior orbital margins. Care was taken at the pedicle area to avoid damage to the pedicle's blood supply. The flap was rotated to position and sutured in layers using polydioxanone suture. (Fig 1 (B & C)) The donor site was closed primarily in cases of small gaps. Generous undermining of the margins in the subgaleal plane was done, followed by closure in layers. On the other hand, dermal grafts were used to cover significant gaps. The graft was taken from the thigh region and sutured in position using a polydioxanone suture.

Medications:

The patients were given a fixed medicinal regimen that includes Enoxaparin 30mg (A low molecular

weight heparin) subcutaneous preoperative injection to reduce the risk of clots in the flap vasculature, Cefotaxime 1gm IV preoperatively and continued every 12 hours for 5 days, Pethidine 50 mg IM preoperatively and every 12 hours for the first day, Hydrocortisone 100mg IV preoperatively, Dexamethasone 4mg IV preoperatively, then continued for six days in a tapering dose regimen (first 2 days q8h, second 2 days q12h+ third 2 days once daily), Alpha-Chymotrypsin 5mg IM preoperatively and continued every 8 hours for 5 days, and Diclofenac sodium 50mg every 8 hours on the second day for 5 days.

Follow up:

Daily wound care was done in the first seven postoperative days. On the 14th postoperative day, pedicle separation was done under local anesthesia. Areas of necrosis were managed with debridement, daily irrigation, and dressing.

Flap monitoring:

Conventional flap monitoring methods were used to evaluate flap viability, including skin color inspection, flap temperature, capillary refill time, and bleeding on puncture. Intraoperative photos were taken using a DSLR camera (Canon 70D) under the operation room light. The photo included the flap and the normal surrounding tissues before flap rotation. One-month postoperative photos were taken to measure flap necrosis.

Chromatic and dimensional analyses:

Intraoperative photos were imported to ImageJ (1.54F) software. The region of interest (ROI) was selected and added to the ROI manager using the polygonal selection tool. ROIs were the normal tissues around the flap incision line (Nr), total flap (FpT), flap base (FpB), flap apex (FpA), flap margins (FpM), and the center of the flap (FpC). (Fig 2 (A & B)) A color histogram was created for each ROI, and the RGB channels' values were exported to an Excel file. Difference of the three light channels of Nr minus FpT (df:Nr-FpT)), FpC minus FpM (df:FpC-FpM), FpB minus FpA (df:FpB-FpA) were calculated. Flap length (FpL), flap base width (FpBW), and flap apex width (FpAW) were measured and exported to the patient Excel file. (Fig 2 (C)) Dimensional ratios were calculated, including FpBW to FpL (FpBW/FpL) and FpBW to FpAW (FpBW/FpAW). One-month postoperative images were imported into the software. The percentage of necrosis area of the flap (%Fp-Nec) method was used to numerically represent the amount of flap necrosis. Using a polygonal selection tool, the entire flap and areas of necrosis were selected and added to the ROI manager. (Fig 2 (D)) Areas of necrosis were summed to determine the total area of flap necrosis (FpNec). %FpNec was calculated using the following equation:[1] (%FpNec = FpNec/FpT X100)

Fig. (1) A: The primary lesion (black arrow). B: Mobilized medial forehead flap. C: Suturing of the median forehead flap to the defect.

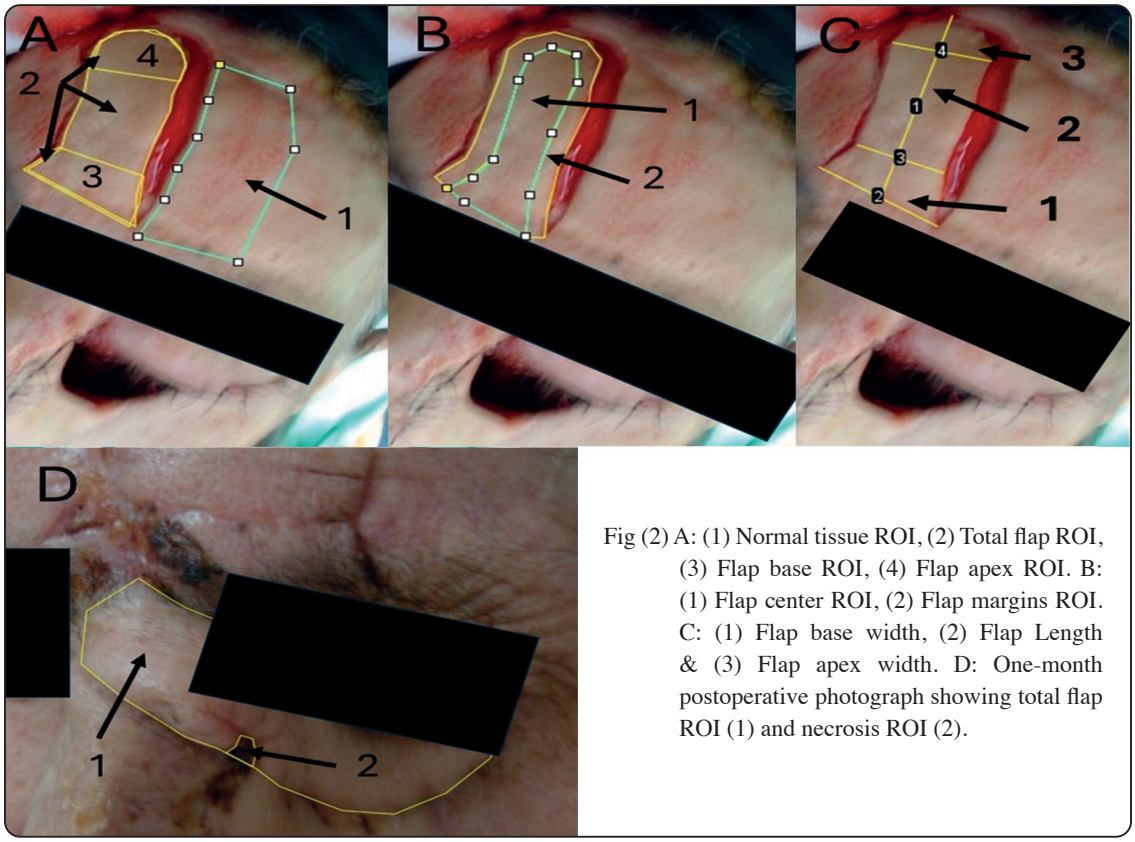

Fig (2) A: (1) Normal tissue ROI, (2) Total flap ROI, (3) Flap base ROI, (4) Flap apex ROI. B: (1) Flap center ROI, (2) Flap margins ROI. C: (1) Flap base width, (2) Flap Length & (3) Flap apex width. D: One-month postoperative photograph showing total flap ROI (1) and necrosis ROI (2).

Statistical analysis:

Mean, standard deviation, and standard error for all measurements were calculated using SPSS software version 25 (IBM). The Shapiro-Wilk test indicated the normality of all data (p-value ranging from 0.932 to 0.081). Hence, parametric tests were used. The Independent sample t-test was used to compare the means of different groups. The effective size was calculated using Cohen's d value. Person's correlation coefficient was used to measure the linear relationship between different ratios and differences. The p-value significance was set at $p<0.05$.

RESULTS

The current study included eight patients (six males and two females) with a mean age of 65. The primary defect in all cases involved part of the cheek and extended to eyelids in some cases and nasal skin in others. (Table 1) None of the cases showed postoperative infection or flap failure. All cases showed different degrees of flap necrosis managed conservatively except for case 5. Case 5 showed three regions of flap necrosis; two were managed conservatively, and one required secondary intervention. (Fig 3 (C & D)) Cases 5 and 2 showed the highest and lowest %FpNec, respectively, which corresponded to the lowest values of FpBW/FpL and FpBW/FpAW for case 5 and the highest values of FpBW/FpL and FpBW/FpAW for case 2. (Table 2) The test of equality of the FpT-Nr, FpB-FpA, and FpC-FpM regarding RGB channels showed no significant differences except for the FpC-FpM green channel. (Table 3)

Interpretation of Cohen's effective size d-value indicated large and medium to practical effects in the tested FpB-FpA for red and green, respectively. Moreover, FpC-FpM showed medium to large practical effects for the RGB values. (Table 4) The person's correlation tests indicated a strong significant inverse relationship between %Fp-Nec and FpBW/FpAW, df:R_FpB-FpA, and df:G_

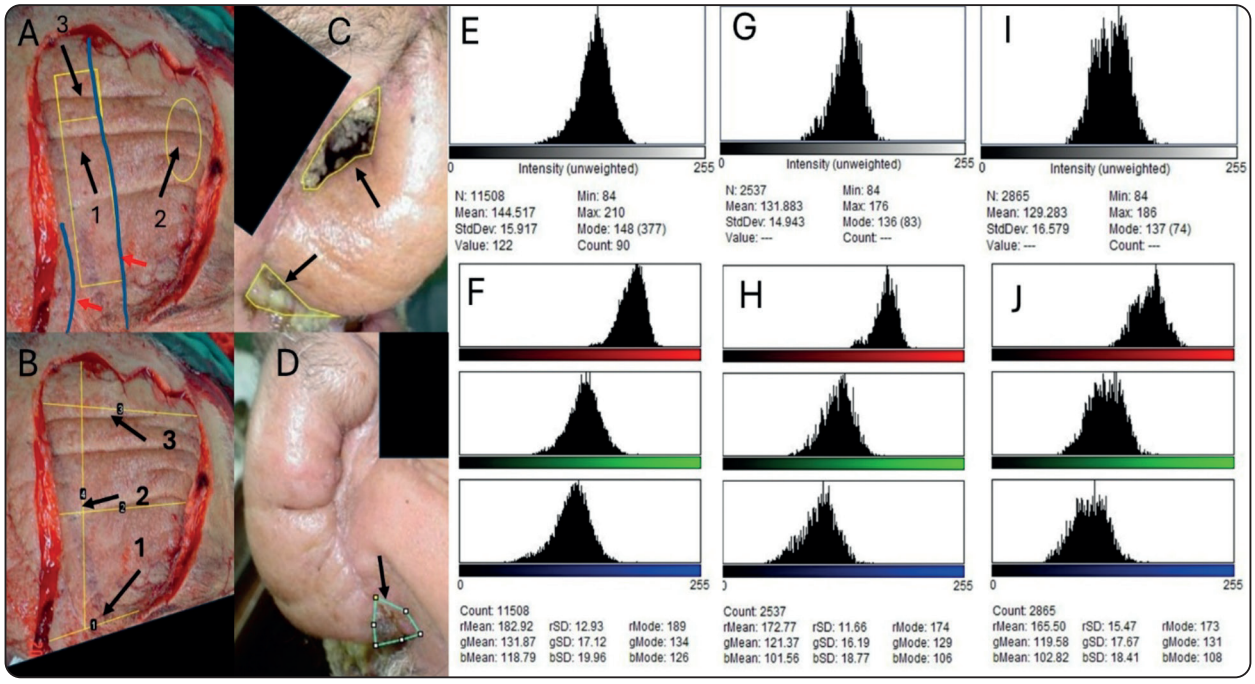

Fig (3) Case No 5 analyses, A: Supratrochlear arteries (red arrows), (1) Total axial segment (including 3), (2) Random segment, (3) Apical part of axial segment. B: (1) Flap base width, (2) Flap length, (3) Flap apex width. C & D: Necrosis regions (black arrows). E & F: Combined and split histogram of total axial segment. G & H: Combined and split histogram of apical part of axial segment. I & J: Combined and split histogram of random segment.

FpB-FpA. At the same time, FpBW/FpAW showed a strong direct relation with df:R_FpB-FpA and df:G_FpB-FpA. In addition, %Fp-Nec showed a strong significant inverse relationship to FpBW/FpL. Meanwhile, FpBW/FpL showed a strong direct correlation to df:R_FpB-FpA. (Table 5)

Case 5 showed the highest %Fp-Nec among cases. Supratrochlear arteries were marked on the flap photo, and then three ROIs were selected representing the total axial, apical axial, and random parts of the flap; ROI histogram and color histogram were created to obtain the combined and split RGB values. The resulting values are presented in Table 6. The axial segment and its apical part showed higher combined and split RGB values than the random ones. (Fig 3)

TABLE (1) Gender distribution and primary lesion sites

Case No	Gender	Primary Lesion Site			
		Cheek	Lower Eyelid	Upper Eyelid	Nasal Skin
1	Male	×	×	×	
2	Male	×	×	×	
3	Male	×			
4	Female	×	×		
5	Male	×			×
6	Male	×			×
7	Male	×	×		
8	Female	×			×

TABLE (2) Means and standard deviations of the %FpNec and flap dimensions ratios

Case No	%FpNec	FpBW/FpL	FpBW/FpAW
1	0.93	0.32	1.36
2	0.77	0.59	1.44
3	8.16	0.39	0.60
4	1.17	0.57	1.40
5	11.56	0.18	0.54
6	4.07	0.29	0.97
7	4.50	0.40	1.05
8	4.47	0.38	0.85
Mean ± StD	4.45 ± 3.80	0.39 ± 0.14	1.03 ± 0.35

TABLE (3) Means and standard deviations of RGB values of different ROIs and test of equality of the calculated differences

Region	Red	Green	Blue
FpT	171.67 ± 13.32	133.49 ± 8.80	122.18 ± 16.51
Nr	167.72 ± 13.32	135.59 ± 8.80	126.08 ± 16.51
FpB	177.53 ± 12.61	133.16 ± 13.17	121.16 ± 20.90
FpA	166.62 ± 13.83	120.48 ± 19.30	110.27 ± 24.66
FpC	175.35 ± 13.88	139.97 ± 11.54	129.21 ± 20.01
FpM	164.07 ± 15.73	124.65 ± 9.32	114.51 ± 15.68

Tested pairs	Color channel	Paired difference				
		M. Diff	Std-EM	95% CI	t-value	Sig.
FpT Nr	Red	3.95	10.58	-18.73 to 26.63	0.374	0.714
	Green	-2.10	8.91	-21.21 to 17.02	-0.235	0.817
	Blue	-3.91	13.25	-32.33 to 24.52	-0.295	0.773
FpB FpA	Red	10.92	6.62	-3.27 to 25.11	1.650	0.121
	Green	12.68	8.26	-5.03 to 30.40	1.536	0.147
	Blue	10.89	11.43	-13.63 to 35.40	0.952	0.357
FpC FpM	Red	11.28	7.42	-4.63 to 27.18	1.520	0.151
	Green	15.32	5.25	4.07 to 26.57	2.921	0.011
	Blue	14.70	9.00	-4.58 to 33.98	1.635	0.124

M. Diff: Mean Difference, Std-EM: Standard Error Mean, CI: Confidence Interval

TABLE (4) Cohen's effective size and their interpretation of the tested pairs regarding RGB channels' values.

Tested pairs	Color channel	T-test Sig.	Effective Size (Cohen's d)	Interpretation
FpT Nr	Red	0.714	0.187	No Practical Effect
	Green	0.817	-0.118	No Practical Effect
	Blue	0.773	-0.147	No Practical Effect
FpB FpA	Red	0.121	0.825	Large Practical Effect
	Green	0.147	0.768	Medium Practical Effect
	Blue	0.357	0.476	Small Practical Effect
FpC FpM	Red	0.151	0.760	Medium Practical Effect
	Green	0.011	1.461	Large Practical Effect
	Blue	0.124	0.818	Large Practical Effect

TABLE (5) Person's correlation tests of %Fp-Nec, FpBW/FpAW, and FpBW/FpL to different variables.

Base Value	Tested Value	Cor Co	Cor L	Sig V	St Sign
%Fp-Nec	df:R_Nr-FpT	-.045	Weak -ve	.92	No
	df:G_Nr-FpT	.103	Weak +ve	.81	No
	df:B_Nr-FpT	-.038	Weak -ve	.93	No
	df:R_FpC-FpM	.554	Moderate +ve	.16	No
	df:G_FpC-FpM	.040	Weak +ve	.93	No
	df:B_FpC-FpM	-.084	Weak -ve	.84	No
	df:R_FpB-FpA	-.953	Strong -ve	.000	Yes
	df:G_FpB-FpA	-.909	Strong -ve	.002	Yes
	df:B_FpB-FpA	-.130	Weak -ve	.76	No
	FpBW/FpL	-.703	Strong -ve	.05	Yes
	FpBW/FpAW	-.951	Strong -ve	.000	Yes
FpBW/FpAW	df:R_FpB-FpA	.951	Strong +ve	.000	Yes
	df:G_FpB-FpA	.820	Strong +ve	.01	Yes
	df:B_FpB-FpA	.077	Weak +ve	.86	No
FpBW/FpL	df:R_FpB-FpA	.703	Strong +ve	.05	Yes
	df:G_FpB-FpA	.554	Moderate +ve	.16	No
	df:B_FpB-FpA	-.490	Moderate -ve	.22	No

Cor Co: Correlation Coefficient, Cor L: Correlation level, Sig V: Significance Value, St Sign: Statistical Significance.

TABLE (6) Axial and random segments combined and split RGB analysis of case 5

ROI	RGB Combined value	R-Value	G-Value	B-Value
Axial Segment Total	144.5±15.9	182.9±12.9	131.9 ±17.1	118.8 ± 20
Axial Segment Apex	131±15	172.8±11.7	121.4 ± 16.2	101.6 ± 18.8
Random Segment	129.38±16.6	165.5± 15.7	119.6 ±17.7	102.8 ± 18.4

DISCUSSION

The region of the head and neck is complex both esthetically and functionally. This applies great demands in reconstruction following facial tumor resection. The median forehead pedicled flap is commonly used to reconstruct significant nasal, orbital, and cheek skin defects.[7] For a long time, researchers were focused on designing the flap pedicle to provide sufficient blood supply essential for flap success. However, analysis of the blood supply of different parts of the flap correlated to flap design and its effect on flap necrosis was not addressed. Flap necrosis, despite flap success, is a crucial complication that has a detrimental impact on facial esthetics that is worth investigating. The ability of chromatic analysis to study the vascularity of different flap parts introduced a simple method to explore and modify flap design to reduce necrosis and improve esthetics.

Flap dimensions showed a significant effect on %Fp-Nec. The difference in red and green channels' values between the flap base and apex strongly correlated with FpBW/FpAW and %Fp-Nec. At the same time, FpBW/FpAW showed a

strong significant relation to the %Fp-Nec. These relations indicate that a wider flap apex than the base increases the risk of flap necrosis. This might be attributed to increased random segments lateral to the axial segment.[36] Choi et al.[37] conducted a study to evaluate the healing of the median forehead flap donor site after primary closure. The flaps were limited to 2cm in width throughout the flap length to reduce problems at the donor sites. This design confined the flap to the axial blood supply, negating random segments. As a result, none of the 42 operated cases showed flap necrosis. Moreover, FpBW/FpL showed a moderate to strong correlation to df:FbB-FpA of the RGB channels, among which df:R_FpB-FpA was statistically significant. This was reflected in the significant strong correlation of %Fp-Nec to FpBW/FpL. These correlations indicate that increasing the FpBW relative to FpL reduced flap necrosis. A study was done by Zhao et al. in 2011[38] on random flaps, indicating a significant increase in flap necrosis with a decrease in FpBW/FpL ratio despite a high success rate of the studied flaps.

Comparison of RGB mean values between FpT-Nr, FpB-FpA, and FpC-FpM showed no statistical significance except for the green channel of FpC-FpM. The high vascularity of the median forehead flaps and the use of low molecular weight heparin preoperatively could explain this. The median forehead flap has blood supply from the broad pedicle at the glabella region, gaining blood supply from both supratrochlear arteries and the terminal branches of the angular artery. Thus, flap blood supply is based on internal and external carotid systems.[10] However, several t-test significances indicate that the differences between groups are close to being significant. Effective size interpretation showed interesting practical effects that warrant further investigations. The comparison between FpB and FpA regarding red and green channels showed moderate to strong practical effects. Moreover, significant practical differences were demonstrated between FpC and FpM regarding RGB channels.

Analyzing the current study result directs attention to the flap dimensions and their relationship with the amount of the axial and random segments of the median forehead flap. Increasing the axial segment of the flap reduces the random segment and, in turn, reduces the effect of increasing flap length relative to base width. The random segments of the flap could be reduced by broadening the base and controlling the flap apex to base widths. This reduces blood supply difference values between the base and apex as well as the center and margins of the flap, reducing flap necrosis. The importance of these flap design parameters was obvious in analyzing case No. 5. Case No. 5 showed the highest %FpNec among the studied cases. One out of three regions of necrosis required a secondary flap for closure. The primary flap was created to reconstruct the entire nasal and medial part of cheek skin; thus, FpAW was nearly double FpBW, and FpL was 5.5 times FpBW. Analyzing combined and split RGB values of the axial and random segments indicated a higher blood supply of the axial part. Moreover, the blood supply of the axial segment's apical part was higher than the random segment's blood supply.

The current study indicated several key points in the median forehead flap design to reduce the risk of flap necrosis. However, this study has potential limitations. The small sample size reduced the statistical significance of some tested values. A larger sample study could increase statistical significance and create indicators to guide the surgeon regarding flap prognosis. The current study used ratios and differences to compare mean values to avoid errors from different image scales and nonuniform ambient light. Uniform imaging scaling and application of custom white balance would aid in standardization. Hence, RGB values could be utilized to create indices for clinical use. Applying chromatic analysis of intraoperative images in detecting flap vascularity is promising.

This technique could be applied to other pedicled flaps to analyze their designs. The simplicity of this technique and the ability to combine it with deep learning modules make it a versatile future research topic.

CONCLUSION

The current study showed that increasing FpBW in relation to FpAW and FpL reduces flap necrosis.

REFERENCES

1. Tim CR, Martignago CCS, et al. A Comparison of Three Methods for the Analysis of Skin Flap Viability: Reliability and Validity. Adv Wound Care (New Rochelle) 2018;7:157-163. DOI: 10.1089/wound.2017.0758
2. Afridi RA, Ahmed E, et al. Demographics of basal cell carcinoma and its surgical management. J Ayub Med Coll Abbottabad 2012;24:141-143.
3. Pfeiffer MJ, Pfeiffer N, et al. Descriptive study on basal cell eyelid carcinoma. Arch Soc Esp Oftalmol 2015;90:426-431. DOI: 10.1016/j.oftal.2014.12.001
4. Armstrong LTD, Magnusson MR, et al. Risk factors for recurrence of facial basal cell carcinoma after surgical excision: A follow-up analysis. J Plast Reconstr Aesthet Surg 2017;70:1738-1745. DOI: 10.1016/j.bjps.2017.04.006
5. Deganello A. Modern oral cavity reconstruction with free flaps and pedicled flaps. J Aesth Reconstr Surg 2015;1:1-5. DOI: https://doi.org/10.4172/2472-1905.100004
6. Mahieu R, Colletti G, et al. Head and neck reconstruction with pedicled flaps in the free flap era. Acta Otorhinolaryngol Ital 2016;36:459-468. DOI: 10.14639/0392-100X-1153
7. Menick FJ. Nasal reconstruction with a forehead flap. Clin Plast Surg 2009;36:443-459. DOI: 10.1016/j.cps.2009.02.015
8. Menick FJ. A 10-year experience in nasal reconstruction with the three-stage forehead flap. Plast Reconstr Surg 2002;109:1839-1855; discussion 1856-1861. DOI: 10.1097/00006534-200205000-00010
9. Kleintjes WG. Forehead anatomy: arterial variations and venous link of the midline forehead flap. J Plast Reconstr Aesthet Surg 2007;60:593-606. DOI: 10.1016/j.bjps.2006.12.006
10. McCarthy JG, Lorenc ZP, et al. The median forehead flap revisited: the blood supply. Plast Reconstr Surg 1985;76:866-869. DOI: 10.1097/00006534-198512000-00012
11. Menick FJ. Aesthetic refinements in use of forehead for nasal reconstruction: the paramedian forehead flap. Clin Plast Surg 1990;17:607-622. DOI: https://doi.org/10.1016/s0094-1298(20)30643-x
12. Politis MJ, Zanakis MF, et al. Enhanced survival of full-thickness skin grafts following the application of DC electrical fields. Plast Reconstr Surg 1989;84:267272. DOI: 10.1097/00006534-198908000-00013
13. Myers MB, Cherry G. Causes of necrosis in pedicle flaps. Plast Reconstr Surg 1968;42:43-50. DOI: https://doi.org/10.1097/00006534-196842010-00008
14. Jones BM. Monitors for the cutaneous microcirculation. Plast Reconstr Surg 1984;73:843-850. DOI: 10.1097/00006534-198405000-00025
15. Khouri RK, Shaw WW. Monitoring of free flaps with surface-temperature recordings: is it reliable? Plast Reconstr Surg 1992;89:495-499. DOI: https://doi.org/10.1097/00006534-199203000-00018
16. Swartz WM, Jones NF, et al. Direct monitoring of microvascular anastomoses with the 20-MHz ultrasonic Doppler probe: an experimental and clinical study. Plast Reconstr Surg 1988;81:149-158. DOI: https://doi.org/10.1097/00006534-198802000-00001
17. Tremper KK. Pulse oximetry. Chest 1989;95:713-715. DOI: https://doi.org/10.1378/chest.95.4.713
18. Oberg PA. Laser-Doppler flowmetry. Crit Rev Biomed Eng 1990;18:125-163.
19. Cervenka B, Bewley AF. Free flap monitoring: a review of the recent literature. Curr Opin Otolaryngol Head Neck Surg 2015;23:393-398. DOI: 10.1097/MOO.0000000000000189
20. Irwin MS, Thorniley MS, et al. Near infra-red spectroscopy: a non-invasive monitor of perfusion and oxygenation within the microcirculation of limbs and flaps. Br J Plast Surg 1995;48:14-22. DOI:10.1016/0007-1226(95)90024-1
21. Kim H, Kwak SH, et al. An Experimental and Clinical Study of Flap Monitoring with an Analysis of the Clinical Course of the Flap Using an Infrared Thermal Camera. Bioengineering (Basel) 2024;11:688. DOI: 10.3390/bioengineering11070688

22. Lee C-E, Chen C-M, et al. A postoperative free flap monitoring system: Circulatory compromise detection based on visible-light image. IEEE Access 2021;10:4649-4665. DOI: https://doi.org/10.1109/access.2021.3136795

23. Offodile AC, 2nd, Chen B, et al. Microporous Polysaccharide Hemospheres Potentiate Ischemia-Induced Skin Flap Necrosis in a Murine Model. Plast Reconstr Surg 2017;139:59e-66e.DOI: 10.1097/PRS.0000000000002907

24. Jia YC, Xu J, et al. The Effect of Atorvastatin on the Viability of Ischemic Skin Flaps in Diabetic Rats. Plast Reconstr Surg 2017;139:425e-433e. DOI: 10.1097/PRS.0000000000002984

25. Lv QB, Gao X, et al. Effects of diammonium glycyrrhizinate on random skin flap survival in rats: An experimental study. Biomed Rep 2016;5:383-389. DOI: 10.3892/br.2016.733

26. Baldan CS, Masson IF, et al. Inhibitory effects of low-level laser therapy on skin-flap survival in a rat model. Plastic Surgery 2015;23:35-39. DOI: https://doi.org/10.4172/plastic-surgery.1000905

27. Nishioka MA, Pinfildi CE, et al. LED (660 nm) and laser (670 nm) use on skin flap viability: angiogenesis and mast cells on transition line. Lasers Med Sci 2012;27:1045-1050. DOI: 10.1007/s10103-011-1042-7

28. Zhou KL, Zhang YH, et al. Effects of calcitriol on random skin flap survival in rats. Sci Rep 2016;6:18945. DOI: 10.1038/srep18945

29. Peng L, Pan X, et al. Natural Hirudin Increases Rat Flap Viability by Anti-Inflammation via PARs/p38/NF-κB Pathway. BioMed Research International 2015;2015:597264. DOI: https://doi.org/10.1155/2015/597264

30. Kashimura T, Soejima K, et al. The Effect of Mature Adipocyte-Derived Dedifferentiated Fat (DFAT) Cells on a Dorsal Skin Flap Model. J Invest Surg 2016;29:6-12. DOI: 10.3109/08941939.2015.1035820

31. Kiranantawat K, Sitpahul N, et al. The first Smartphone application for microsurgery monitoring: SilpaRamanitor. Plast Reconstr Surg 2014;134:130-139. DOI: 10.1097/PRS.0000000000000276

32. Takiwaki H. Measurement of skin color: practical application and theoretical considerations. J Med Invest 1998;44:121-126.

33. Brinca A, Pinho A, et al. Searching for a mathematical model for blood perfusion of random pattern skin flaps: a clinical pilot study using in vivo laser speckle contrast imaging. J Eur Acad Dermatol Venereol 2018;32:e406-e409. DOI: 10.1111/jdv.14997

34. Lister T, Wright PA, et al. Optical properties of human skin. J Biomed Opt 2012;17:090901. DOI: 10.1117/1.JBO.17.9.090901

35. Gu J, Tomioka Y, et al. Measurement of optical reflection and temperature changes after blood occlusion using a wearable device. Sci Rep 2020;10:1-13. DOI: 10.1038/s41598-020-68152-6

36. Richards A, Dafydd H. General Principles. In: Richards A, Dafydd H (eds). Key Notes on Plastic Surgery, 2014:1-79. DOI: https://doi.org/10.1002/9781118757017.ch1

37. Choi JS, Bae YC, et al. Evaluation of the donor site after the median forehead flap. Arch Plast Surg 2018;45:259-265. DOI: 10.5999/aps.2017.01277

38. Zhao T, Yu D, et al. Experimental study on the relationship between the ratio of length to width of slender narrow pedicle and random flap survival area in pig. Chinese Journal of Plastic Surgery 2011;27:40-43.